Available online at www.sciencedirect.com

SCIENCE DIRECT®

Journal of Applied Geophysics 56 (2004) 247–261

JOURNAL OF APPLIED GEOPHYSICS

www.elsevier.com/locate/jappgeo

Optimizing a layered and laterally constrained 2D inversion of resistivity data using Broyden's update and 1D derivatives

Anders V. Christiansen*, Esben Auken

The Hydrogeophysics Group, Department of Earth Sciences, University of Aarhus, Finlandsgade 6-8, 8200 Aarhus N, Denmark

Received 20 August 2003; accepted 6 July 2004

Abstract

Dense profile-oriented resistivity data allows for 2D and 3D inversions. However, huge amounts of data make it practically impossible to do full 2D or 3D inversions on a routine basis. Therefore, a number of approximations have been suggested over the years to speed up computations. We suggest using a combination of Broyden's update on the Jacobian matrix with derivatives calculated using a 1D formulation on a parameterized 2D model of locally 1D layered models. The approximations bring down the effective number of 2D forward responses to a minimum, which again gives us the ability to invert very large sections. Broyden's update is not as useful with a parameterized problem as is the case with a smooth minimum structure problem that has been the usual application. 1D derivatives, however, seem to be very effective when initiating a full 2D solution with Broyden's update. We compare the different methods using two different kinds of data on two synthetic models and on two field examples. The most effective and reliable optimization combines 1D derivatives with a full 2D solution and Broyden's update. When using Broyden's update the Jacobian matrix needs to be reset every once in a while. We do this whenever the difference in data residual from the previous iteration is less than 5%. This combined inversion method reduces the computation time approximately a factor of 3 without losing model resolution.

Keywords: Inversion; 2D; DC resistivity; Optimizations; Broyden's update; 1D derivatives

1. Introduction

Standard electrical methods allow for a detailed mapping of the subsurface by gathering profile-oriented data continuously with large sensitivity overlaps between individual data points (e.g. Dahlin, 1996; Bernstone and Dahlin, 1999; Sørensen, 1996; Panissod et al., 1997). Some of the systems in use produce huge amounts of data in a field day (more than 20,000 data points). With the dense data coverage provided, 2D and 3D interpretations are of course desirable. However, most 2D and certainly any 3D inversion code utilizing full forward and inverse

* Corresponding author.
E-mail addresses: anders.vest@geo.au.dk (A.V. Christiansen), esben.auken@geo.au.dk (E. Auken).
URL: http://www.hgg.au.dk.

0926-9851/$ - see front matter © 2004 Elsevier B.V. All rights reserved.
doi:10.1016/j.jappgeo.2004.07.004

solutions become increasingly slower with larger data sets.

Standard 2D inversion algorithms have been presented by, e.g., Oldenburg and Li (1994) and Loke and Barker (1996), both producing smooth minimum structure models in which sharp formation boundaries are hard to recognize. A few inversion programs have been suggested that produce blocky or layered models. Olayinka and Yaramanci (2000) presented a 2D block-type inversion scheme using polygons of equal resistivity. Smith et al. (1999) presented a layered inversion scheme with lateral constraints on resistivities and depths applied to magnetotelluric (MT) data. Auken and Christiansen (2004) have adapted the model description of Smith et al. (1999) and used it in a 2D inversion scheme for resistivity data which produces laterally smooth models with discrete layers.

Approximations to a full solution for an inversion algorithm can be done on several stages in the forward solution, in the calculation of derivatives or in the inverse matrix manipulations. However, the savings in computation time is obtained at the expense of the loss of accuracy which is the inevitable consequence of numerical approximations. Thus, there is a trade-of between the savings in computation time and the required accuracy.

Loke and Barker (1996) suggested a quasi-Newton formulation which gave major time reductions using Broyden's update formula (Broyden, 1965). The quasi-Newton method has been widely used with success in smooth minimum structure 2D resistivity inversions. Oldenburg and Ellis (1991) introduced approximate inverse mappings in both the model space (AIM-MS) and in the data space (AIM-DS). They exemplified the AIM-DS with the 2D MT problem using a 1D formulation as an approximate inverse. This proved powerful with MT data. The Rapid Relaxation Inverse (RRI) by Smith and Booker (1991) also combined 2D and 1D formulations for the MT problem. In the RRI, the derivatives are 1D except for the fact that they comply with the 2D fields. An extremely fast multichannel deconvolution (MCD) on resistivity data was suggested by Møller et al. (2001), where the output is a smooth picture of the subsurface resistivity distribution obtained without direct computation of the 2D fields. Torres-Verdín et al. (2000) used a smaller grid as an approximate 2D finite-difference forward, incorporated in an auxiliary inversion scheme. This inversion method is in many ways similar to the AIM-DS presented by Oldenburg and Ellis (1991) only the approximate inverse is not a 1D formulation but a 2D formulation using a smaller grid.

This paper combines Broyden's update formula with derivatives calculated using a composite 1D formulation along the profile taking advantage of a piecewise 1D model description. The 1D derivatives are used for the first few iterations while the model is still in is infant stages without too much 2D structure. Later, a full 2D iteration is computed followed by iterations taking advantage of Broyden's update formula. For the resistivity problem, 1D calculations are magnitudes of order faster than 2D calculations. Thus, introducing 1D calculations reduces computation times compared to solutions using only 2D calculations.

2. Inversion methodology

The inversion is based on an algorithm developed for a laterally constrained 1D inversion scheme (1D-LCI) (Sørensen et al., 2004). The 1D-LCI was expanded to cover the 2D case as well by including a 2D forward response in the inversion algorithm (Auken and Christiansen, 2004). A detailed description of the basics of the inversion methodology is found in Auken and Christiansen (2004) from which we in this section will give a brief summary presenting the key concepts and basic equations.

2.1. Data and model

Consider a resistivity profile with n_x reference node points, x_i, in the horizontal direction. For each node point, we have an ordinary data vector, $\mathbf{d}_i$, of apparent resistivity observations for several different electrode spreads. The whole profile section shall be modelled as one inverse problem, and hence the relevant data vector is the concatenation of the data at each node:

$$\mathbf{d}_{\text{obs}} = (\mathbf{d}_1, \mathbf{d}_2, \ldots, \mathbf{d}_{nx})^T, \tag{1}$$

here T indicates the vector transpose. For a simple continuous vertical electrical sounding (CVES) profile, the grouping of the data vector is sketched in Fig. 1.

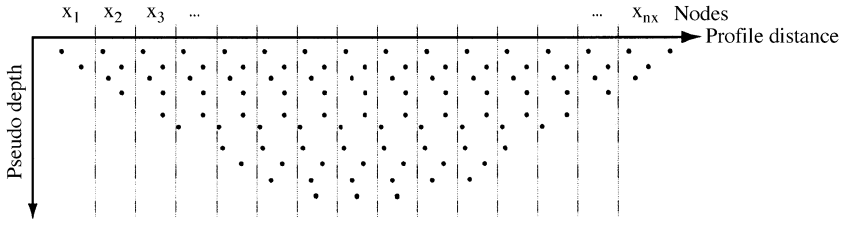

Fig. 1. Data grouping. The individual four-pole configurations are grouped into soundings based on the lateral position of their focus point.

To minimize non-linearity and to impose positivity, we apply logarithmic data and logarithmic parameters (e.g. Johansen, 1977; Ward and Hohmann, 1988). Hence

$$\mathbf{d}_i = \left(\log(\rho_{a_1}), \log(\rho_{a_2}), \ldots, \log(\rho_{a_{Ni}})\right)^T, \quad (2)$$

where ρ_a denotes apparent resistivity and N_i is the number of electrode configurations measured at x_i.

At each surface node, x_i, the subsurface model is represented by a logarithmic 1D model with n_1 layers

$$\mathbf{m}_i = \Big(\log(\rho_{i1}), \log(\rho_{i2}), \ldots, \log\left(\rho_{in_1}\right), \log(t_{i1}), \log(t_{i2}), \ldots, \log\left(t_{i(n_1-1)}\right)\Big)^T, \quad (3)$$

where ρ denotes interval resistivity and t denotes interval thickness. The total number of submodels is n_x corresponding to the number of individual 1D soundings. Each submodel is described by n_1 layers, so the full model

$$\mathbf{m} = \begin{pmatrix} \mathbf{m}_1 \\ \mathbf{m}_2 \\ \vdots \\ \mathbf{m}_{n_x} \end{pmatrix}, \quad (4)$$

to be determined has $M=n_x*(2n_1-1)$ parameters.

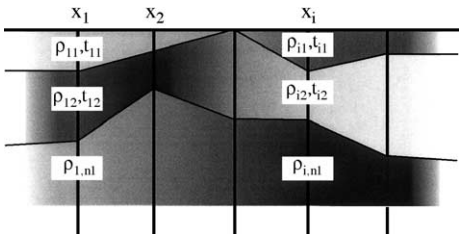

Fig. 2. Model description. The model is described with thicknesses and resistivities at a number of nodes along a profile. The parameters between neighboring nodes are linearly interpolated to produce a 2D model.

To produce the 2D model from the composite 1D profile, parameters from neighbouring nodes are interpolated linearly as illustrated in Fig. 2.

Thus, locally we have a 1D model description which in combination builds the full 2D profile. Grouping the data vector according to the model setup enables mixing of 1D and 2D calculations.

2.2. Forward modeling

The 2D resistivity forward modeling in the inversion routine is performed using the finite difference code from University of British Columbia (McGillivray, 1992). The code uses a finite difference approach similar to the one described by Dey and Morrison (1979).

The layered 2D model is translated to the finite difference grid by superimposing the grid on the model and assigning a resistivity value to each cell based on an area weighted average of the contributing elements in the underlying layered 2D model, see Fig. 3.

Electrodes are placed on node points in the grid. For electrodes not on node points, we have implemented a linear interpolation to the electrode positions involving the two nearest nodes.

2.3. Forward mapping

The dependence of apparent resistivities on subsurface parameters is in general described as a non-linear differentiable forward mapping. We follow the established practice of linearized approximation by the first term of the Taylor expansion

$$\mathbf{d}_{\text{obs}} \cong \mathbf{g}(\mathbf{m}_{\text{ref}}) + \mathbf{G}(\mathbf{m}_{\text{true}} - \mathbf{m}_{\text{ref}}) + \mathbf{e}_{\text{obs}}, \quad (5)$$

where $\mathbf{g}$ is the nonlinear forward mapping of the model to the data space and $\mathbf{e}_{\text{obs}}$ is the error on the

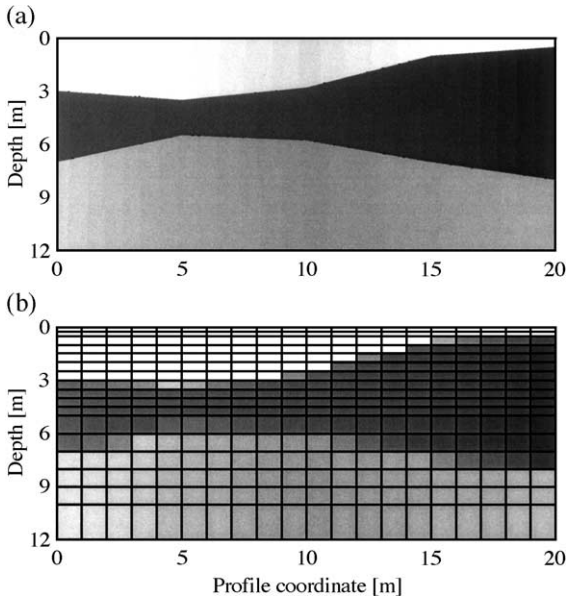

Fig. 3. Model translation. The layered model in (a) is translated to the model superimposed on the finite difference grid in (b) using weighted averages.

observed data. The true model, $\mathbf{m}_{\text{true}}$, has to be sufficiently close to some arbitrary reference model, $\mathbf{m}_{\text{ref}}$, for the linear approximation to be a good one. In short, we write:

$$\delta\mathbf{d}_{\text{obs}} = \mathbf{G}\delta\mathbf{m}_{\text{true}} + \mathbf{e}_{\text{obs}}, \tag{6}$$

where $\delta\mathbf{d}_{\text{obs}}=\mathbf{d}_{\text{obs}}-\mathbf{g}(\mathbf{m}_{\text{ref}})$. The Jacobian, $\mathbf{G}$, contains all the partial derivatives of the mapping

$$G_{\text{st}} = \frac{\partial d_{\text{s}}}{\partial m_{\text{t}}} = \frac{\partial \log(\rho_{a_{\text{s}}})}{\partial \log(m_{\text{t}})} = \frac{m_{\text{t}}}{\rho_{a_{\text{s}}}} \frac{\partial \rho_{a_{\text{s}}}}{\partial m_{\text{t}}}, \tag{7}$$

for the s-th apparent resistivity in the data vector and the t-th parameter in the model vector.

2.4. Prior information and lateral constraints

Prior information, which is used to resolve ambiguities and to add, e.g., geological information, can be added at any point of the profile and migrates through the lateral constraints to adjacent models. The models are tied together laterally by introducing lateral constraints between neighboring parameters. This means that information from models with a small variance migrates through the lateral bands to models with higher variance. The code utilizes lateral constraints on resistivities, thicknesses and depths. For most applications, lateral constraints on depths are advantageous to constraints on thicknesses. Constraints on depths are preferred in cases where there is a demand for continuity of layer boundaries, e.g., a Quaternary sequence with sand and clay layers on top of a relatively smooth pre-Quaternary surface. Constraints on thicknesses are favourable whenever there is a possibility of discontinuous layer boundaries, but continuous thicknesses, e.g., across a fault. In this paper, constraints are applied to resistivities and depths.

The lateral constraints and prior information enters the vector with observed data, and derivatives are calculated to enter the Jacobian matrix, $\mathbf{G}$. The practical implementation of prior information and lateral constraints can be reviewed in Auken and Christiansen (2004).

2.5. Inversion

With the prior information and the lateral constraints added to the data vector, $\mathbf{d}'$, and the corresponding derivatives added to the Jacobian matrix, $\mathbf{G}'$, we write Eq. (6) compactly as:

$$\mathbf{G}'\delta\mathbf{m}_{\text{true}} = \delta\mathbf{d}' + \mathbf{e}' \tag{8}$$

The joint observation error is $\mathbf{e}'$, with covariance matrix $\mathbf{C}'$.

The model estimate (Menke, 1989)

$$\delta\mathbf{m}_{\text{est}} = \left(\mathbf{G}'^{T}\mathbf{C}'^{-1}\mathbf{G}'\right)^{-1}\mathbf{G}'^{T}\mathbf{C}'^{-1}\delta\mathbf{d}', \tag{9}$$

minimizes

$$Q = \left(\frac{1}{N+A+M}\sum_{i=1}^{N+A+M}\left[\frac{\delta\mathbf{d}'^{\,2}_{i}}{\text{var}(\mathbf{e}'_{i})}\right]\right)^{\frac{1}{2}} \tag{10}$$

where N is the number of data, A is the number of constraints and M is the number of model parameters, including depths.

Currently, the matrix operations in Eq. (9) is solved using a Cholesky decomposition (Press et al., 1992), which implies that for very large models (more than about 5000 model parameters) the matrix calculations can be very time consuming because the computations

are proportional to M^3, where M is the number of model parameters. For such big systems, it is beneficial to use a sparse solution as, e.g., described in Akin (1982).

2.6. Data acquisition systems

The examples given later are based on two different resistivity systems. The CVES consists of a number of steel electrodes manually forced into the ground at regular electrode spacing, typically from 2 to 12 m (Van Overmeeren and Ritsema, 1988; Dahlin, 1996). The electrodes function as both current and potential electrodes and can measure in any configuration desired by the user. The data collecting is semi-continuous using a roll-along technique.

The pulled array continuous electrical sounding (PACES) system consists of a small tractor, equipped with processing electronics, pulling the electrodes mounted on a tail (Sørensen, 1996). The electrodes are cylindrical steel tubes with a weight of about 15 kg. Two electrodes are maintained as current electrodes, while the remaining electrodes serve as potential electrodes in eight different configurations. The data collecting is continuous at a speed of approximately 1.5 m/s with one full sounding saved each second. The data are later processed to one sounding for every 5.0 m.

3. Optimizations

3.1. Forward calculations with a sliding model window

Long profiles or systems with irregular electrode configurations inevitably mean large finite difference grids. This can make it practically impossible to calculate full forward responses with one large grid. Instead, we split up the profile in model windows and do calculations for one window at the time sliding it along the profile. Afterwards, the responses from the windows (dark gray) are concatenated to create the full profile, as illustrated in Fig. 4a.

Experimentally, we found the computation time to depend linearly on $n^2\log_2(n)$ for n cells, when the number of vertical nodes has be chosen appropriately. This is an approximation, because the computation time depends differently on the number of cells in the

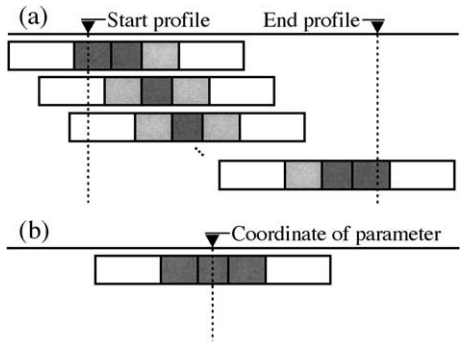

Fig. 4. Sliding model window. (a) shows the sliding model windows for forward responses, whereas (b) is for derivatives. Light gray and dark gray are the fine parts of the grid. Electrodes need to be within the fine parts of the grid with the lateral focus point in the dark gray. The light gray are overlaps between the sliding model windows and have to be sufficiently large to ensure continuous forward responses when concatenating the full response of the dark gray sections. White areas are padding.

two directions. Also, the number of current electrodes needs to be taken into account, but for profiles up to 3 km the correlation is very good. Thus, an optimal choice of the size of the sliding model window can reduce the computation time drastically. A large sliding model window means fewer but computationally more expensive computations, whereas a small sliding model window means more but faster computations. The overlap between neighboring model windows (light gray) always needs to be sufficiently large in order to ensure continuous forward data along the profile. The sizes of the overlap, the padding zones (white) and the number of vertical nodes are fixed when appropriate values have been determined for the actual configuration. The sizes of these fixed grid values depend primarily on the configurations used, but also on the geology of the survey area. Ideally, the fixed sizes are therefore determined from scratch for each survey, based on forward calculations of an expected geophysical model, ensuring continuous forward data along the concatenated profile. The overlap should be at least 0.5 times the maximum layout, but a subsurface with strong 2D features would most likely require overlaps of more than 1 times the maximum layouts. In this paper, the required overlap has been established from forward calculations and it is between 0.65 and 0.9 times the maximum layouts. The accuracy using the sliding model window is in these case better that 1%

compared to the response calculated without the sliding model window.

However, besides these fixed configuration dependent parameters the grid can be optimized in terms of the size of the central sliding window (SW) (dark gray in Figs. 4 and 5). Fig. 5 shows the relative timing of two different configurations on a 1100-m profile, assuming a $n^2\log_2(n)$ dependence.

Fig. 5a shows the relative timing of a 400-m CVES layout with 5 m between horizontal grid points in the fine part. In this case, the layout is quite large compared to the profile length and there is no time gained using the slider. The shortest computation time is achieved when choosing the SW to be 400 m bringing the total size of the fine grid to 1100 m (400 m+2*70*5 m) equal to the profile length.

In Fig. 5b, the same profile is measured with the PACES system (Sørensen, 1996), which has approximately 90-m layout and the horizontal grid size is 1 m. For the PACES system, the optimal size of the SW is 140 m (i.e. 140 cells), which is almost three times as fast as if the full profile where computed with just one grid. A longer profile would have made the time saving even larger.

The sliding model window can also be used to speed up calculations of derivatives taking advantage of the fact that derivatives for a certain parameter have the highest values for configurations close to the parameter itself. Thus, we calculate derivatives with only one window, centering this at the lateral position of the parameter in question as depicted in Fig. 4b. Doing this we need to take special care designing the grid for the sliding window. If it is too small we leave out derivatives that would have contributed to the 2D description. Making the grid very large only enhances accuracy, but might bring unnecessary computations since the derivatives for data far away from the parameter is close to zero anyway.

In this paper, we have used the slider throughout, with the same sizes of the sliding model window used for calculation of derivatives and for forward calculations. Though, we will use the name "full 2D" when both the forward calculations and the calculations of derivatives are performed using a 2D formulation even though the sliding model window have been used.

3.2. Broyden's update

Broyden's update formula (Broyden, 1965) has been used widely for 2D resistivity inversion. The update formula approximates the Jacobian matrix, $\mathbf{G}_{n+1}$, of iteration n+1 using the Jacobian matrix of iteration n:

$$\mathbf{G}_{n+1}\mathbf{B}_{n+1} = \mathbf{B}_n + [\Delta\mathbf{d}_n - \mathbf{B}_n\Delta\mathbf{m}_n]\frac{\Delta\mathbf{m}_n^T}{\Delta\mathbf{m}_n^T\Delta\mathbf{m}_n}, \quad (11)$$

where $\mathbf{B}$ is referred to as the Broyden matrix and

$$\Delta\mathbf{d}_n = \mathbf{d}_n - \mathbf{d}_{n-1},$$

$$\Delta\mathbf{m}_n = \mathbf{m}_n - \mathbf{m}_{n-1}. \quad (12)$$

The update formula is based on an assumption that the difference in forward mappings, $\Delta\mathbf{d}(\mathbf{m}_n)$, changes

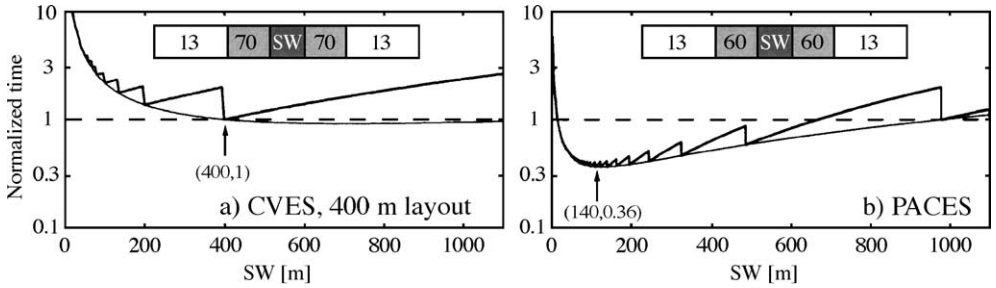

Fig. 5. Optimizing the sliding model window. (a) shows a 1100-m CVES profile with a 400-m layout (largest electrode separation) and 5-m horizontal grid size. (b) shows a 1100-m PACES profile (approx. 90-m layout) with 1-m grid. Numbers in the boxes are the number of horizontal grid points in each separate part. The thick solid line is the normalized computation time, relative to the time using just one grid, for varying sizes of the central SW. The line is jagged because only a whole number of sliding windows is possible. The thin solid line is the underlying function permitting fractions of sliding windows.

linearly with respect to $\mathbf{m}_n$, in the direction of $\Delta\mathbf{m}_n$. This is most likely to be the case close to the maximum of the least squares cost-function.

Most of the previous implementations have been in smooth minimum structure programs (e.g., Loke and Barker, 1996). The cell based finite-difference or finite-element implementation of the forward problem in these programs imply that only resistivities are inverted for. When parameterizing the problem into, for example, thicknesses and resistivities of discrete layers we introduce a mixture of physical parameters and structure. Several authors have noted that the forward mapping in this case is more linearly dependent on the physical parameters than on the structure. Torres-Verdín et al. (2000), implemented Broyden's update formula on a parameterized cross-borehole problem. They experienced a need to reset the entries in the Jacobian matrix after a few iterations, doing the full, time consuming solution. Otherwise the problem did not converge. This is not the case with the minimum structure solutions. Loke and Dahlin (2002) found that if the Jacobian matrix is initiated and perhaps fully recalculated for the first two or three iterations the final model will be very close to the full Gauss–Newton model.

Based on these considerations, we have implemented Broyden's update formula with an option to reset and recalculate the Jacobian if necessary. As the criterion to recalculate the full Jacobian matrix, we use the change in data residual between the latest two iterations. The value is defined by the user, but to our experience 5–10% seems to be suitable.

3.3. 1D derivatives

The derivatives in the Jacobian matrix of Eq. (7) are approximated by a first-order forward-difference formula:

$$\frac{\partial d_s}{\partial m_t} = \frac{g_s(m_t + \Delta m_t) - g_s(m_t)}{\Delta m_t}, \tag{13}$$

where Δm_t is chosen as small as possible (1–2% of m). This implementation requires at least one forward calculation per model parameter and one forward per model. In the parameterized 2D case this means M+1 forward calculations, which is very time consuming for large problems. Instead, we suggest calculating the entries to the Jacobian matrix with a 1D forward mapping (1D derivatives). For the 1D resistivity case, a forward calculation is extremely fast, practically eliminating the Jacobian calculation as a time factor. Only the data from individual soundings corresponding to the grouping of the model vector now contribute to the total **G**-matrix making this a block-diagonal:

$$\mathbf{G} = \begin{bmatrix} \left\{\frac{\partial d}{\partial m}\big|_{x=x1}\right\} & & & \underline{\underline{0}} \\ & \left\{\frac{\partial d}{\partial m}\big|_{x=x2}\right\} & & \\ & & \ddots & \\ \underline{\underline{0}} & & & \left\{\frac{\partial d}{\partial m}\big|_{x=xn_x}\right\} \end{bmatrix} \tag{14}$$

for the n_x models with n_x data sets.

For one iteration, we now need to do only one full 2D calculation on the model from the previous iteration and n_x 1D calculations to fill the Jacobian matrix, **G**. For a subsurface resistivity structure close to a 1D model, this will work fine. For very complex 2D structures, the approximation will be poor, since the off-diagonal elements in the 2D **G**-matrix will have non-negligible values compared to the bloc-diagonal elements.

The first-order forward-difference formula in Eq. (13) is crude, but an easy way to calculate derivatives. Faster solutions could be implemented, such as the adjoint method (McGillivray and Oldenburg, 1990), which has been widely used for smooth minimum structure inversion of resistivity data.

3.4. Combining Broyden's update and 1D derivatives

Since we now have the full 1D solution, the full 2D solution, 1D derivatives with 2D forward and Broyden's update incorporated in the inversion scheme an obvious solution is to do a combination to make an optimal solution in terms of speed and accuracy.

Normally, the iterative solution is started with a homogeneous halfspace. This means that very little 2D information is present in the beginning. Based on this fact, we have chosen to start the inversion procedure with 1D derivatives in conjunction with 2D forward, at some point switching to doing a few full 2D iterations to initiate the entries of the 2D

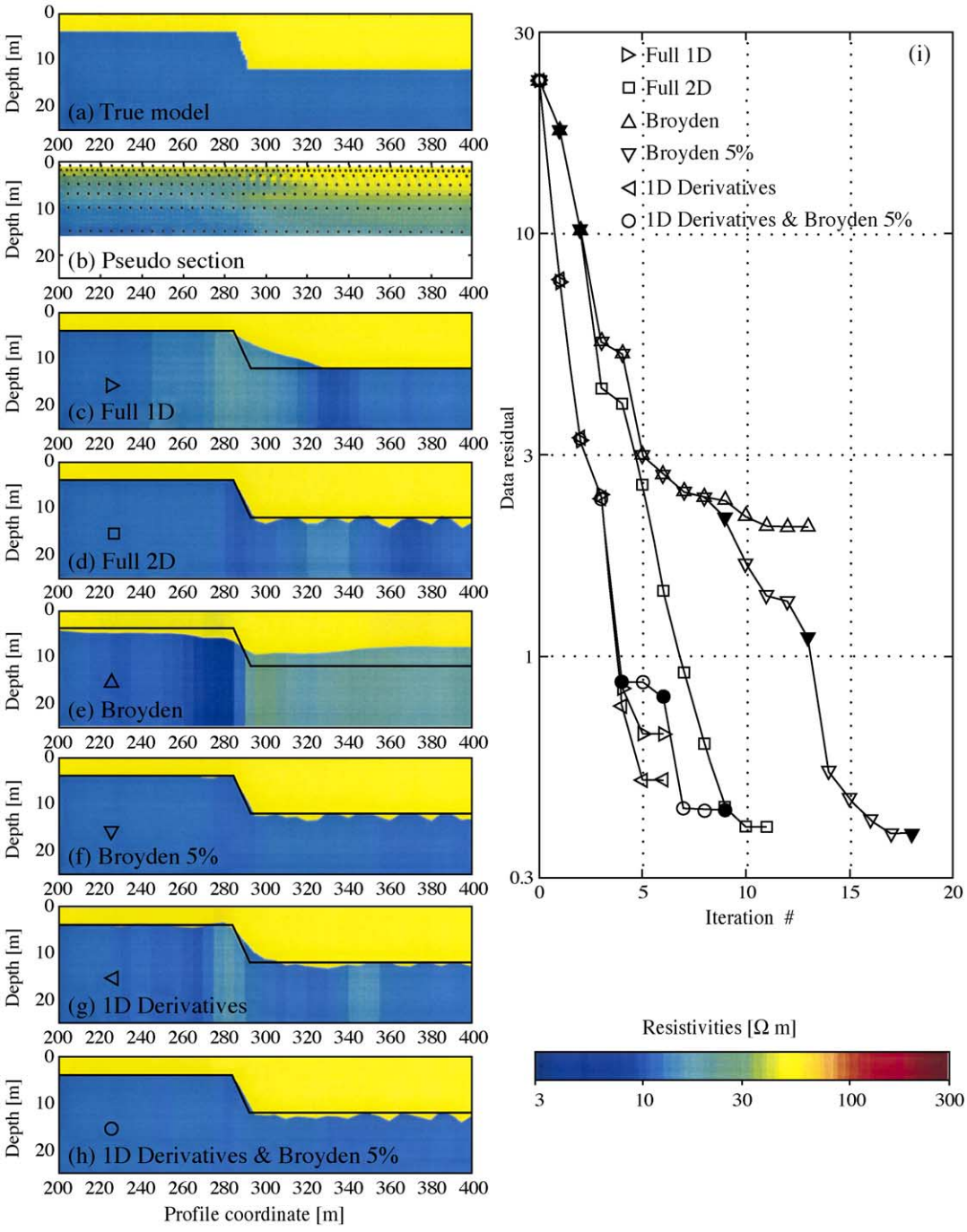

Fig. 6. Synthetic PACES example. Panel (a) is the true model. Panel (b) is a pseudo-section of the data. Panel (c) is the model from a full 1D inversion; (d) is the result using a full 2D solution. Panel (e) presents an inversion using Broyden's update formula for all iterations except the .rst two. Panel (f) also uses Broyden's update formula, but the full Jacobian is recalculated when the residual change is less than 5%. The model in panel (g) is the result of 1D derivatives throughout. Panel (h) combines 1D derivatives with the full 2D solution and Broyden's update formula. Finally, the data residuals are presented in (i) as a function of iteration number. Filled markers (for Broyden 5% and 1D derivatives+Broyden 5%) indicate full 2D iteration.

Jacobian matrix, finally switching to Broyden's update. If the subsurface is thought to be fairly 1D, the 1D derivatives can be exchanged with the full 1D solution, i.e. exchanging the 2D forward with a 1D forward. Generally, this iteration scheme should minimize the number of full 2D solutions while keeping as much 2D information as possible. Also, the Broyden solution should be stabilized because the model misfit will be closer to the desired misfit minimum, minimizing nonlinearity errors.

4. Synthetic examples

4.1. Simple dip-model, PACES data

The first example in Fig. 6a is a very simple two-layer model with a 45° descending slope on the lower layer. The data set is generated using the PACES electrode configuration (Sørensen, 1996), with one sounding per meter, each comprising 8 data points. The synthetic forward data were produced using the DCIP2D software, from University of British Colombia (McGillivray, 1992). The 5% noise was added to the data, which were then processed to one sounding per 5 m as if they were field data. The profile is 600 m long with 960 data points in 120 models (660 model parameters).

The panels on the left side of Fig. 6 (panels a–g) presents various inversions using 1D, 2D, Broyden's update, 1D derivatives and a combination of Broyden's update and 1D derivatives. The plots on the right side (Fig. 6i) are the corresponding data residuals for each iteration. Panel (c) presents a full 1D inversion which clearly does not resolve the 2D slope. Panel (d) is the full 2D solution, which finds the correct geometry except for the wiggles on the deep parts of the conductive layer due to noisy data and decreasing resolution. Panel (e) presents the solution using Broyden's update for all iterations after initiating the inversion with two full 2D iterations. From the model section and the residual plot on the right, it is clear that Broyden's update as stand-alone does not converge to a satisfactory model. Panel (f) is Broyden's update with full 2D recalculation of the Jacobian whenever the change in data residual is less than 5%. The model now converges towards the true model, but more iterations are needed compared to the full 2D solution. Panel (g) is the solution using 1D derivatives for all iterations. Iteration for iteration the residual of this method follows the residual of the 1D solution (Fig. 6i) except for the last two iterations, indicating that the 2D structures are found at the very last iterations. The final model is in between the model from the full 2D solution (Fig. 6d) and the model from the full 1D solution (Fig. 6c). Finally, panel (h) presents the combination of 1D derivatives with a Broyden's update on successive iterations. 1D derivatives were carried out for the first four iterations, then one full 2D solution and finally Broyden's update with the 5% criterion.

The timing of the examples in Fig. 6 is summarized in Table 1. The total CPU time is given in column 1, with the number of full 2D iterations in column 2. All inversions are tested on a 2.8-GHz Pentium4 processor.

The primary time consumer in this case is clearly the 2D iterations. For larger problems, the time taken to do the matrix calculations can be significant as well, although it can be minimized taking advantage of fairly sparse matrices.

From this simple synthetic example, we conclude that Broyden's update by itself is not applicable for parameterized problems. If combined with full 2D updates of the Jacobian matrix convergence is assured. Using 1D derivatives works quite well with this simple geometry and combining them with a full 2D solution using Broyden's update speeds up the computation time without losing 2D information. However, for more complex structures, the 1D derivatives as stand-alone is insufficient and we will not show these results in the following examples. Results from the full 1D solution will not be shown either.

Table 1
Summary of computation times and number of full 2D iterations for the inversions presented in Fig. 6

Method	Computation time (s)	Number of iterations	Number of full 2D iterations
(c) Full 1D	5	6	0
(d) Full 2D	8779	11	11
(e) Broyden	1627	13	2
(f) Broyden 5%	4397	18	5
(g) 1D derivatives	284	6	0
(h) 1D derivatives and Broyden 5%	2415	9	3

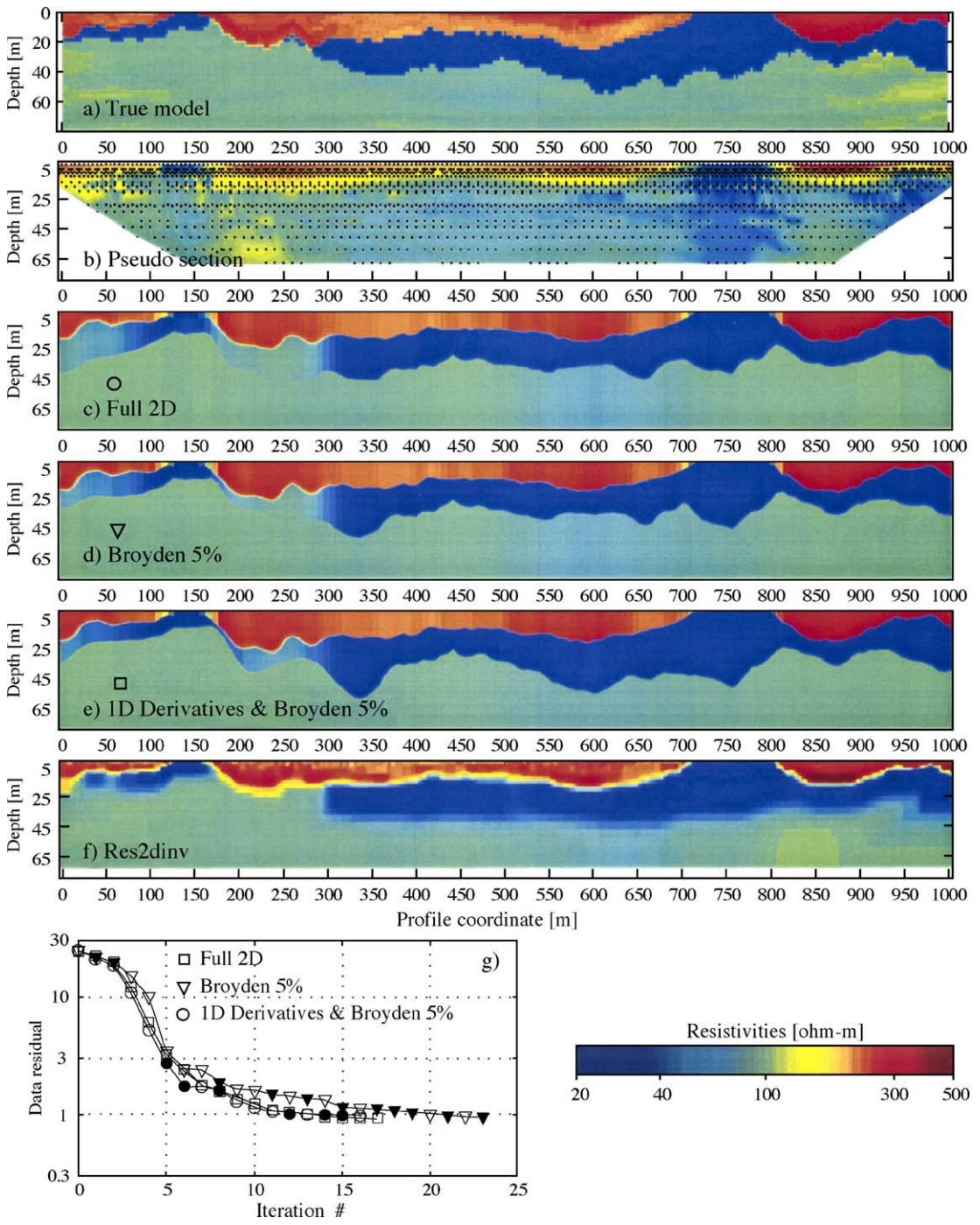

Fig. 7. Von-Karman synthetic model. Panel (a) is the true model, panel (b) is the pseudo-section, panel (c) is the full 2D solution, and panel (d) uses Broyden's update formula with a 5% recalculation criteria. Panel (e) combines 1D derivatives with a 5% Broyden's update. Panel (f) shows the result from the Res2dinv program for comparison and, finally, the data residuals versus iteration number are displayed in (g). Filled markers (for Broyden 5% and 1D derivatives+Broyden 5%) indicate full 2D solution.

4.2. Von-Karman model, CVES, continuous gradient array

The three-layered model (Fig. 7a) is made from a stationary stochastic process. The degree of spatial correlation is parameterized in terms of the fractal dimension of a self-affine process, which is characterized by the von Karman covariance functions (Møller et al., 2001; Serban and Jacobsen, 2001). The synthetic model is made in a "sedimentary" way, i.e., first layer (bottom layer) is deposited as a homogeneous halfspace; first layer is eroded; second layer is deposited (draped) on top of the eroded surface of the first layer; erosion of first and second layer unit; third layer (top layer) deposited on top of eroded surface. Average resistivities are 300 Ω m (top layer), 30 Ω m (middle layer) and 100 Ω m. The standard deviation on the layer resistivities is 0.3 times the logarithm to the average values.

The data are generated using the CVES system in a continuous gradient array configuration. The number of data is approximately twice the number of data collected with traditional Wenner arrays, and it has proven to be superior in resolving non-horizontal earth structures (Dahlin and Zhou, 2002). The 3555 data points are collected for a profile 1 km long with a minimum electrode distance of 5 m. The model has 215 surface node points each described by 3 layers, totally 1075 model parameters.

More complex models would have needed four layers to produce a satisfying model, but in this case three layers are sufficient.

Both the full 2D (Fig. 7c), the 2D and Broyden 5% (Fig. 7d) and the combination of 1D, 2D and Broyden 5% (Fig. 7e) identifies the major units and structures in the true model, but differs in the details. For some parts of the model, more layers are present than is needed to describe the true model (e.g., around coordinate 200–300 m). This causes soft transitions in both resistivities and layer boundaries. If any information on the prior geological appearance of the measuring site is present, these transitions can be controlled by the settings of the lateral constraints. Thus, if the lateral constraints on depths are tighter than the constraints on resistivities, transitions will mostly take place as changes in resistivity with constant layer boundaries and vice versa. In these examples, we have tried to maintain average settings allowing both changes in resistivity and layer boundaries. The result from Res2dinv (Fig. 7f) (Loke and Barker, 1996) is rather similar to the layered results although the lower boundary is not as accurately resolved.

Table 2
Summary of computation times and number of full 2D iterations for the inversions presented in Fig. 7

Method	Computation time (s)	Number of iterations	Number of full 2D Iterations
(c) Full 2D	32,339	17	17
(d) Broyden 5%	20,158	23	11
(e) 1D derivatives and Broyden 5%	12,381	16	7
(f) Res2dinv	12,532	8	2

The residual curves (Fig. 7g) follow very identical paths, but the Broyden 5% is somewhat slower to converge, and thus needs more iterations. All models fit the data to the same degree.

The timings of the models in Fig. 7 are summarized in Table 2. This example is rather large in terms of data as well as model parameters explaining the rather large computation times. Also it is worth noticing that more iterations are needed for convergence compared to the previous simple dip model.

We timed this data set with the Res2dinv as well. Setting recalculation of the Jacobian for the first two iterations, this data set was inverted in 12,532 s doing eight iterations. This is comparable to the 12,381 s we used in the optimized solution. Christiansen and Auken (2003) showed that for a variety of synthetic examples the 2D-LCI performed equally well as Res2dinv comparing the inverted models point-to-point.

5. Field examples

5.1. PACES, groundwater survey, Denmark

The PACES system has been used widely in Denmark for hydrogeological mapping (Sørensen et al., 2004). The line presented here is a small part of a 29 km^2 campaign with a total of 113 km of PACES profile. The profile is 1 km long with one sounding containing 8 data points every 5 m. The

model is described at 201 nodes, totally 1005 model parameters (3 layers). The data noise is assumed to be 5%.

The resulting models (Fig. 8b,c,d) have a high resistive layer over a more conductive layer with a more resistive layer at the bottom. The model responses of the Broyden 5% (Fig. 8c) and Broyden 5% combined with 1D derivatives (Fig. 8d) are very similar and they are quite similar to the full 2D result (Fig. 8b) as well.

The accumulated thickness of clay layers is the primary target of most PACES surveys because they form protective covers over potential groundwater reservoirs. Identifying "windows" in the clay layer is also very important. In the example above, the clay layer is the middle low-resistive layer found for the entire profile except the very last part after profile coordinate 950 m.

The timing of the PACES field examples is summarized in Table 3. In this case, the 1D

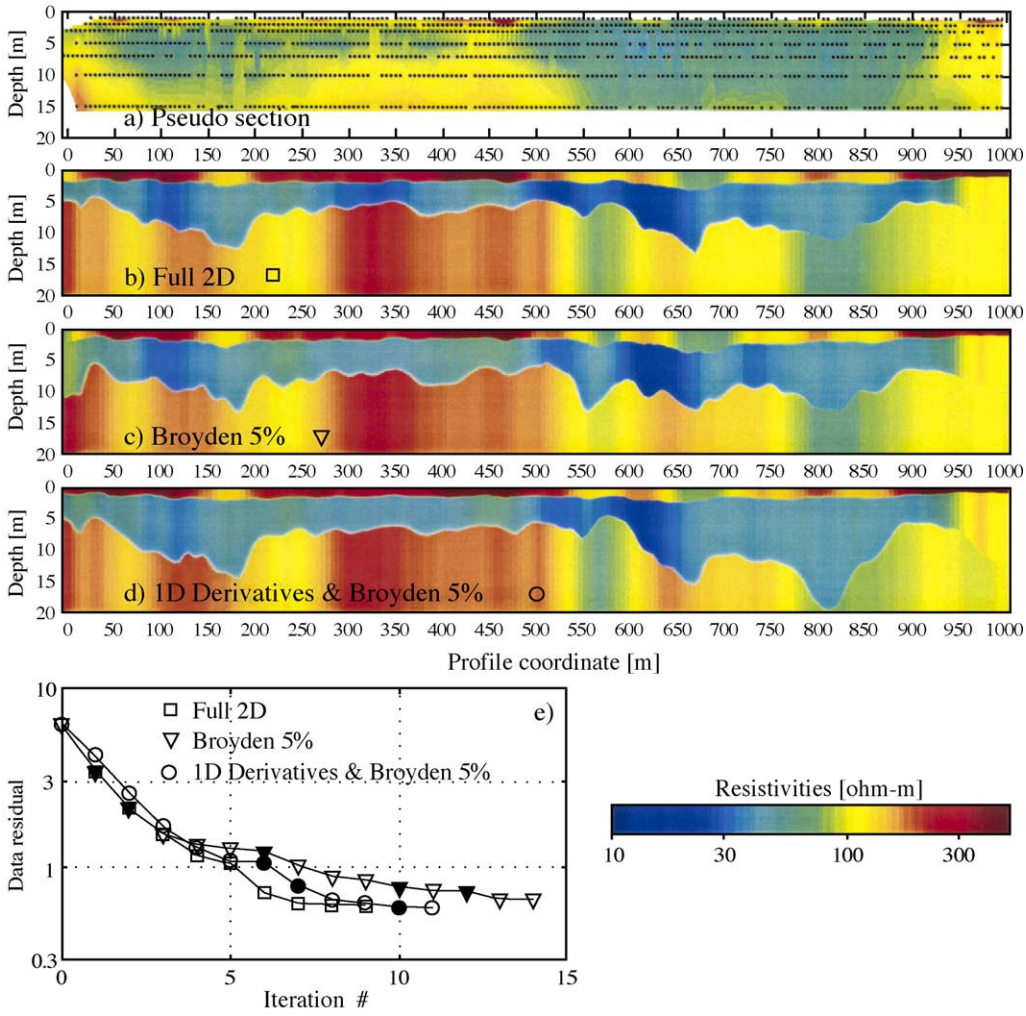

Fig. 8. PACES field example. Panel (a) is the data pseudo section, panel (b) is the full 2D solution, and panel (c) uses Broyden's update formula with a 5% recalculation criteria. Panel (d) combines 1D derivatives with a 5% Broyden's update. Finally, the data residuals versus iteration number are plotted in (e). Filled markers (for Broyden 5% and 1D derivatives+Broyden 5%) indicate full 2D solution.

Table 3
Summary of computation times and number of full 2D iterations for the inversions presented in Fig. 8

Method	Computation time (s)	Number of iterations	Number of full 2D Iterations
(b) Full 2D	14,089	9	9
(c) Broyden 5%	8301	14	5
(d) 1D derivatives and Broyden 5%	4760	11	3

derivatives+Broyden 5% reduces the computation time by approximately a factor of 3.

5.2. CVES, road construction, Sweden

The next field example is a CVES data set from Sweden. The profile is approximately 300 m. The resistivity survey was carried out as part of the geotechnical investigations for road construction in connection with a filled basin structure in bedrock. The data set consists of 536 data points measured with a CVES system using Wenner configurations with a-distances from 2 to 48 m. The data noise is assumed to be 5%. The data set has previously been presented by Dahlin (1996) and in Auken and Christiansen (2004). The model has 71 horizontal nodes each with 4 layers, totally 497 model parameters.

The model results from the different inversions are practically the same. Minor differences are obtained in the outer lower parts of the profile where practically no information is present, as depicted by the pseudo section (Fig. 9a). All models correlated well with the information from the drillings, which identifies three distinct units in the small basin. These units are very hard to distinguish using traditional smooth minimum structure inversion (Dahlin, 1996). Between coordinate 20 and 100,

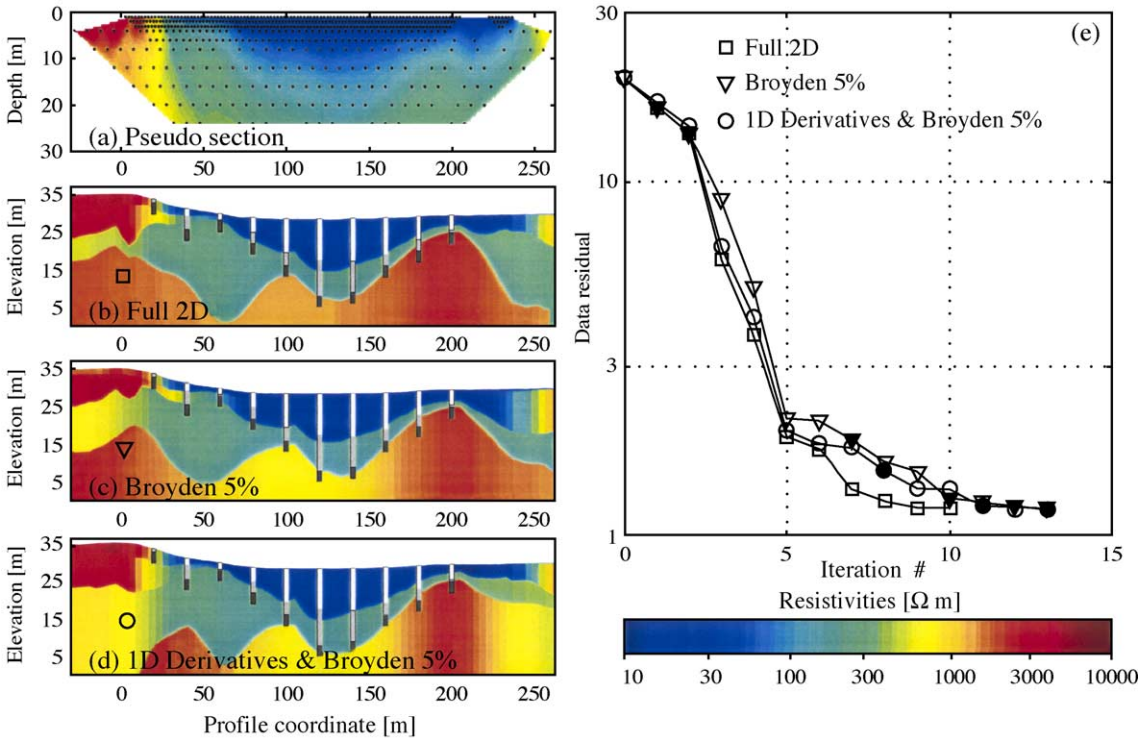

Fig. 9. CVES field example. Panel (a) is the data pseudo section, panel (b) is the full 2D solution, and panel (c) uses Broyden's update formula with a 5% recalculation criteria. Panel (d) combines 1D derivatives with a 5% Broyden's update. Finally, the data residuals versus iteration number are plotted in (e). Filled markers (for Broyden 5% and 1D derivatives+Broyden 5%) indicate full 2D solution. Lithological logs from drillings are located at every 20 m from coordinate 20 to 200 m. The colors of the drill holes indicate from the bottom: rock (dark gray), till (light gray) and clay (white).

Table 4
Summary of computation times and number of full 2D iterations for the inversions presented in Fig. 9

Method	Computation time (s)	Number of iterations	Number of full 2D Iterations
(b) Full 2D	9891	10	10
(c) Broyden 5%	5074	13	5
(d) 1D derivatives and Broyden 5%	3291	13	3

there is less agreement between drill information and models, probably due to 3D effects associated with the basin edge.

The timing in Table 4 shows that the combination of 1D derivatives with Broyden's update brings the effective number of full 2D solutions down to only three which is very acceptable compared to the 10 needed if no approximations are used.

6. Discussion

In all the examples given here, it makes good sense to use either of the approximations suggested, but for all cases the combination of 1D derivatives with a Broyden's update had the shortest computation time and thus recommends itself. However, models with strong 2D features would most likely be difficult to optimize using the 1D derivatives solution in which cases either the full 2D or the 2D with Broyden 5% should be used.

Extremely large data sets can be practically impossible to invert even with the approximate solutions suggested here. Normally, a full 1D solution would be the alternate choice, but instead we suggest to use 1D derivatives throughout producing an intermediate result between the 1D and the 2D solutions.

Another way to optimize the 2D-LCI is to shortcut the first couple of iterations by producing a suitable starting model. This can be done with the multi-channel deconvolution as suggested by Møller et al. (2001). Having produced a smooth deconvolved 2D model we only need to find the best fitting layered models along the profile and use those as starting models.

Finally, one could implement a dual-grid method because the size of the grid used in the finite element or finite difference calculations affects computation times dramatically. Thus, applying a fine grid for forward calculations and a coarser grid for calculation of derivatives could speed up computations (Torres-Verdín et al., 2000).

7. Conclusion

The 2D-LCI is a method utilizing a layered model description for 2D resistivity inversion. The models and data are grouped into pairs of soundings and models along the profile. This enables mixtures of 2D and 1D inversions. The parameters in the 2D-LCI are regularized using lateral constraints on layer resistivities, thicknesses and/or depths, producing laterally smooth models with discrete layers.

We have presented the use of 1D derivatives and Broyden's update with a 2D layered inversion of profile resistivity data. Broyden's update as stand-alone is not usable with this kind of problem. To ensure convergence the Jacobian matrix needs to be reset using a full 2D solution every once in a while. We have used a 5% relative change in residual between the last two iterations as a criteria to update the Jacobian. Some of the speed gained using Broyden's update is lost, but it is still approximately twice as fast as the full 2D solution.

Calculation of the Jacobian matrix using a 1D mapping instead of a 2D forward mapping practically eliminates the Jacobian calculation as a time factor. However, the Jacobian becomes a block-diagonal containing no 2D information and it is only applicable for relatively smooth 2D earth structures. Used as a starter for a 2D Broyden's update inversion scheme it proved very useful because very little 2D information is present in the first few iterations.

The inversions with 1D derivatives are very fast because only one full 2D forward calculation is needed for every iteration and they can be used as stand-alone for extremely large data sets where 2D solutions are not applicable. Whenever the 2D earth structures are not too strong we suggest using the inversion scheme combining 1D derivatives with a full 2D solution and Broyden's update. The computation time for this inversion scheme were reduced by

approximately a factor 3 compared to the full 2D solution.

Acknowledgements

The field data were kindly provided by Prof. Torleif Dahlin, University of Lund, Sweden. We would also like to thank Prof. Douglas Oldenburg at University of British Columbia for letting us use their 2D resistivity code in our implementation.

References

Akin, J.E., 1982. Application and Implementation of Finite Element Methods. Computational Mathematics and Applications Series. Academic Press.

Auken, E., Christiansen, A.V., 2004. Layered and laterally constrained 2D inversion of resistivity data. Geophysics 69, 752–761.

Bernstone, C., Dahlin, T., 1999. Assessment of two automated DC resistivity data acquisition systems for landfill location surveys: two case studies. Journal of Environmental & Engineering Geophysics 4 (2), 113–121.

Broyden, C.G., 1965. A class of methods for solving nonlinear simultaneous equations. Mathematics of Computation 19, 577–593.

Christiansen, A.V., Auken, E., 2003. Layered 2-D inversion of profile data, evaluated using stochastic models. Proceedings volume, 3DEM-III, February 2003, Adelaide.

Dahlin, T., 1996. 2D resistivity surveying for environmental and engineering applications. First Break 14 (7), 275–283.

Dahlin, T., Zhou, B., 2002. Gradient and mid-point referred measurements for multi-channel 2D resistivity imaging. Proceedings, Integrated Case Histories Session, Proceedings of the 8th Meeting EEGS-ES, Aveiro, Portugal.

Dey, A., Morrison, H.F., 1979. Resistivity modeling for arbitrarily shaped 2-dimensional structures. Geophysical Prospecting 27, 106–136.

Johansen, H.K., 1977. A man/computer interpretation system for resistivity soundings over a horizontally stratified earth. Geophysical Prospecting 25, 667–691.

Loke, M.H., Barker, R.D., 1996. Rapid least squares inversion of apparent resistivity pseudosections by a quasi-Newton method. Geophysical Prospecting 44, 131–152.

Loke, M.H., Dahlin, T., 2002. A comparison of the Gauss–Newton and quasi-Newton methods in resistivity imaging inversion. Journal of Applied Geophysics 49, 149–162.

McGillivray, P.R., 1992. Forward modeling and inversion of DC resistivity and MMR data. PhD thesis, University of British Columbia, Vancouver, Canada.

McGillivray, P.R., Oldenburg, D.W., 1990. Methods for calculating fréchet derivatives and sensitivities for the non-linear inverse problem: a comparative study. Geophysical Prospecting 38, 499–524.

Menke, William, 1989. Geophysical Data Analysis—Discrete Inverse Theory. (Rev. ed.). International Geophysics Series. Academic Press, San Diego.

Møller, I., Jacobsen, B.H., Christensen, N.B., 2001. Rapid inversion of 2-D geoelectrical data by multi-channel deconvolution. Geophysics 66, 800–808.

Olayinka, A.I., Yaramanci, U., 2000. Use of block inversion in the 2-D interpretation of apparent resistivity data and its comparison with smooth inversion. Journal of Applied Geophysics 45, 63–81.

Oldenburg, D.W., Ellis, R.G., 1991. Inversion of geophysical data using an approximate inverse mapping. Geophysical Journal International 105, 325–353.

Oldenburg, D.W., Li, Y., 1994. Inversion of induced polarization data. Geophysics 59, 1327–1341.

Panissod, C., Lajarthe, M., Tabbagh, A., 1997. Potential focusing: a new multielectrode array concept, simulating study, and field tests in archaeological prospecting. Geophysics 38, 1–23.

Press, W.H., Teukolsky, S.A., Vetterling, W.T., Flannery, B.P., 1992. The Art of Scientific Computing, Numerical Recipes, vol. 2. Cambridge University Press, Cambridge, pp. 1–963.

Serban, D.Z., Jacobsen, B.H., 2001. The use of broad-band prior covariance for inverse palaeoclimate estimation. Geophysical Journal International 147, 29–40.

Smith, J.T., Booker, J.R., 1991. Rapid inversion of two and three-dimensional magnetotelluric data. Journal of Geophysical Research 96, 3905–3922.

Smith, T., Hoversten, M., Gasperikova, E., Morrison, F., 1999. Sharp boundary inversion of 2D magnetotelluric data. Geophysical Prospecting 47, 469–486.

Sørensen, K.I., 1996. Pulled array continuous electrical profiling. First Break 14, 85–90.

Sørensen, K.I., Auken, E., Christensen, N.B., Pellerin, L., 2004. An Integrated Approach for Hydrogeophysical Investigations: New Technologies and a Case History, Accepted for publication in SEG, NSG Vol II: Applications and Case Histories.

Torres-Verdín, C., Druskin, V., Fang, S., Knizhnerman, L.A., Malinverno, A., 2000. A dual-grid nonlinear inversion technique with applications to the interpretation of dc resistivity data. Geophysics 65, 1733–1745.

Van Overmeeren, R.A., Ritsema, I.L., 1988. Continuous vertical electrical sounding. First Break 6, 313–324.

Ward, S.H., Hohmann, G.W., 1988. Electromagnetic theory for geophysical applications. Nabighian, M.N. Electromagnetic Methods in Applied Geophysics vol. 1[4]. Society of exploration geophysicists (SEG). Investigations in geophysics. Neitzel, E.B., Tulsa, pp. 131–311.